


EAP45 association with budding HIV-1: Kinetics and domain requirements

Bo Meng¹ | Pedro P. Vallejo Ramirez² | Katharina M. Scherer² |
Ezra Bruggeman² | Julia C. Kenyon^{1,3,4} | Clemens F. Kaminski² |
Andrew M. Lever^{1,5} 

¹Department of Medicine, University of Cambridge, Addenbrooke's Hospital, Cambridge, UK

²Laser Analytics Group, Department of Chemical Engineering and Biotechnology, University of Cambridge, Cambridge, UK

³Department of Microbiology and Immunology, National University of Singapore, Singapore, Singapore

⁴Homerton College, University of Cambridge, Cambridge, UK

⁵Department of Medicine, National University of Singapore, Singapore, Singapore

Correspondence

Clemens F. Kaminski, Laser Analytics Group,
Department of Chemical Engineering and
Biotechnology, University of Cambridge,
Cambridge, UK.

Email: cfk23@cam.ac.uk

Andrew M. Lever, Department of Medicine,
University of Cambridge, Addenbrooke's
Hospital, Cambridge, UK.

Email: amll1@medschl.cam.ac.uk

Funding information

Engineering and Physical Sciences Research
Council, Grant/Award Numbers: EP/
H018301/1, EP/L015889/1; Gates Cambridge
Scholarship; Infinitus China Ltd; Medical
Research Council, Grant/Award Numbers: MR/
K015850/1, MR/K02292X/1, MR/
N0229939/1; MedImmune; Microbiology
Society; RCUK Technology Touching Life
Initiative; Wellcome Trust, Grant/Award
Numbers: 089703/Z/09/Z, 203249/Z/16/Z

Abstract

A number of viruses including HIV use the ESCRT system to bud from the infected cell. We have previously confirmed biochemically that ESCRT-II is involved in this process in HIV-1 and have defined the molecular domains that are important for this. Here, using SNAP-tag fluorescent labelling and both fixed and live cell imaging we show that the ESCRT-II component EAP45 colocalises with the HIV protein Gag at the plasma membrane in a temporal and quantitative manner, similar to that previously shown for ALIX and Gag. We show evidence that a proportion of EAP45 may be packaged within virions, and we confirm the importance of the N terminus of EAP45 and specifically the H0 domain in this process. By contrast, the Glue domain of EAP45 is more critical for recruitment during cytokinesis, emphasising that viruses have ways of recruiting cellular components that may be distinct from those used by some cellular processes. This raises the prospect of selective interference with the pathway to inhibit viral function while leaving cellular functions relatively unperturbed.

KEYWORDS

budding, colocalisation, ESCRT, gag, HIV, TIRF

1 | INTRODUCTION

ESCRTs (endosomal sorting complexes required for transport) are protein complexes involved in a variety of cellular functions, from the

scission of the intercellular bridge during cytokinesis, to the formation of multi-vesicular bodies (MVB) and the extracellular budding of a number of viruses including human immunodeficiency virus (HIV). ESCRT activities involve the topological remodelling of membranous

Bo Meng and Pedro P. Vallejo Ramirez contributed equally to this work.

This is an open access article under the terms of the Creative Commons Attribution License, which permits use, distribution and reproduction in any medium, provided the original work is properly cited.

© 2021 The Authors. *Traffic* published by John Wiley & Sons Ltd.

structures. The core of the ESCRT machinery comprises ESCRT-I (TSG101 [Vps23], VPS28, VPS37, and MVB12/UBAP1), -II (EAP20 (Vps25), EAP30 (Vps22), and EAP45 (Vps36)) and -III (CHMP1-7) acting in a sequentially coordinated manner during membrane scission.¹ The ESCRT machinery also has two other associated complexes, ESCRT-0 which precedes early cargo recruitment, and VPS4 AAA ATPase/VTA1 which universally act at a late stage for membrane scission.²

Many viruses take advantage of the properties of the ESCRTs during their life cycle. In the case of HIV, a small number of Gag polyproteins form oligomers in the cytosol, possibly with the genomic RNA, before they are trafficked to the plasma membrane where further Gag molecules nucleate and membrane deformation occurs.³⁻⁵ Budding occurs at specific microdomains at the plasma membrane enriched in lipid 'raft' associated components which are recognised as sites of ESCRT protein accumulation.^{3,6}

Two late domains within the p6 domain of Gag, with the motifs PTAP and YPXL, interact with the ESCRT-I protein TSG101 and the ESCRT-associated protein ALIX, respectively, which then recruit ESCRT-III for the final scission to occur.³ Our understanding of the recruitment of the ESCRTs during Gag accumulation at the membrane has benefitted from biochemical analyses of budding events,⁷⁻¹⁰ as well as from advanced fluorescence microscopy techniques which have examined the temporal dynamics of these events.¹¹⁻¹⁴ Interestingly, TSG101 and ALIX show different dynamics once engaged with Gag; TSG101 co-occurs with Gag as Gag multimerises,^{15,16} whereas ALIX is only recruited when Gag puncta reach maximum intensity.¹⁴ ESCRT-III components are recruited to the budding site and remain there for 3-5 minutes¹¹ with recent data indicating recurrent transient recruitment of CHMP4B and VPS4 until successful cleavage occurs.^{5,17} Because of the transitory nature of these recruitments, the temporal co-occurrence between various components of ESCRT with Gag is very low, with only ~1% to 4% of the total Gag at the plasma membrane detectably colocalised with an ESCRT component, as measured by direct stochastic optical reconstruction microscopy (dSTORM).¹⁸

Extensive work has been carried out in elucidating the function of ESCRT-I and ESCRT-III in HIV budding and in other cellular processes,¹⁹ however the role of ESCRT-II is still emerging. ESCRT-II comprises one copy of EAP30 and EAP45 (Figure 1A) and two copies of EAP20 together forming a Y shaped structure.²⁰ Structural studies in yeast show ESCRT-I interacts with ESCRT-II via the C-terminal domain (CTD) of Vps28 and the N terminus of the Vps36 (EAP45 in metazoans) Glue and H0 linker domains^{1,20,21} (Figure 1A). A homologous region in mammalian EAP45 was also shown to interact with TSG101 by yeast two-hybrid screening.²² The remaining domains of EAP45 (WH1 and WH2) and EAP30 form the core structure of the ESCRT-II complex with EAP20,^{20,23} which is responsible for recruiting ESCRT-III,²⁰ though an alternative link is also documented.²⁴ Although ESCRT-II's role as the canonical bridge in linking to ESCRT-I in MVB formation²⁵⁻²⁷ and cytokinesis is established,²⁴ the same role has been controversial in HIV budding. An earlier siRNA knockdown (KD) study of EAP20 suggested ESCRT-II is dispensable for HIV budding in 293T cells,²² however, the ESCRT-II complex was shown to be required for the recruitment of ESCRT-III at the HIV assembly site in a

reconstitution system *in vitro*.²⁸ Our recent study using CRISPR/EAP45 knockout (KO) HAP1 and T cells showed that EAP45 is required for efficient HIV budding and spreading.^{29,30} The specificity of this effect was demonstrated by the ability of EAP45 *in trans* to rescue the EAP45 KO cell-mediated virus budding and by its dependency on the H0 linker region for interacting with ESCRT-I.³⁰ The discrepancy between these studies may have arisen from minor amounts of residual ESCRT-II in the siRNA KD study still being sufficient for functional budding. Interestingly, cell proliferation was largely unperturbed by the depletion of EAP45 and yet there was up to a 10-fold decrease in virus spreading, suggesting that EAP45 is redundant for cell growth but is critical for viral multiplication and spread.³⁰ This, together with the apparent requirement for early ESCRT proteins to ensure the specific recruitment of the Gag-Pol polyprotein,³⁰ underlines the importance of understanding the mechanistic roles of ESCRT-II in HIV budding. Further insights into these protein-protein interactions could help in developing a new class of antivirals to treat HIV.

In addition to its link with ESCRT-I in viral budding, the Glue domain in EAP45 contains ubiquitin-binding and lipid-binding sites for membrane anchoring at the endosome.^{31,32} It was shown in yeast that neither phosphatidylinositol 3-phosphate (PI3P) nor ubiquitin-binding sites are required for endosomal anchoring of Vps36 but the link to ESCRT-I is.²⁵ In metazoans, the Glue domain is believed to be involved in the recruitment of EAP45 at the endosomal membrane, presumably because of its multifaceted roles.³² However, direct visual evidence for this is lacking.

Building on our previous biochemical evidence supporting the role of ESCRT-II in HIV budding, here we used a SNAP-tag to label EAP45 and employed widefield total internal reflection fluorescence (TIRF)³³ microscopy to visualise and quantify its spatial colocalisation, or co-occurrence, with HIV Gag polyprotein at the plasma membrane in fixed cells. Furthermore, we used single particle tracking in live HeLa cells to study the dynamics of the interaction between EAP45 and Gag. We used this labelling approach to compare the HIV utilisation of EAP45 with those of endosomal membrane recruitment and cytokinesis. We find variations in the domain requirements of EAP45 in these processes that may have therapeutic potential.

2 | RESULTS

2.1 | Fusion of a SNAP tag at the N terminus of EAP45 does not affect its normal cellular localisation

The SNAP tag (~20 kDa) is derived from the mammalian DNA repair protein O⁶-alkylguanine-DNA alkyltransferase and is widely used for imaging studies on both fixed and live cells because of the versatility of the commercially available substrates, providing a superior specificity for targeting the protein of interest.³⁴ A slightly bigger GFP tag (~27 kDa) was previously inserted at the N terminus of EAP45 without adversely affecting its cellular localisation³² so we decided to SNAP label EAP45 at the same site (Figure 1A). Overexpression of ESCRT protein can sometimes have adverse effects on cells.^{7,8} To

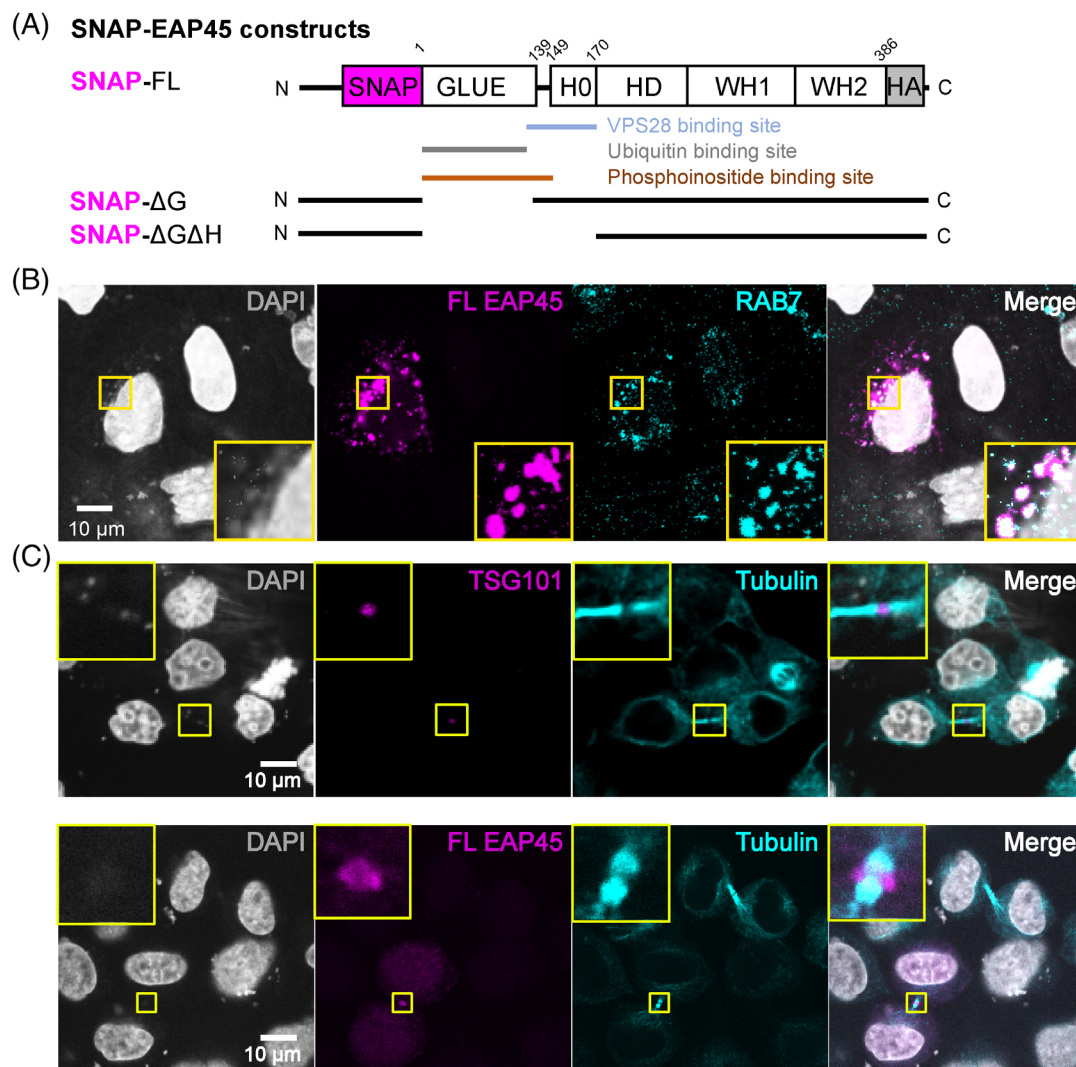


FIGURE 1 Verification of the SNAP-tag labelling for EAP45 in endosomal localisation and cytokinesis. A, Schematic diagram showing EAP45 constructs labelled with a SNAP tag at the N terminus and an HA tag at the C terminus used in this study. The known interacting domains are highlighted underneath. B, Confocal images of HeLa cells transfected with SNAP-FL EAP45 constructs and stained 1 day post-transfection with DAPI for nuclei, RAB7 for late endosomes and AlexaFluor647 conjugated SNAP substrates for EAP45. C, Confocal images of HeLa cells constitutively expressing YFP-TSG101 stained with DAPI for nuclei and α -tubulin show that TSG101 is recruited to the intercellular bridge (upper panels). Confocal images of HeLa cells transfected with SNAP-FL EAP45 followed by staining with DAPI, α -tubulin and Alexa647 conjugated SNAP substrate also show EAP45 is recruited to the intercellular bridge during cytokinesis (lower panels). Close-up views in yellow insets in this figure and throughout this study highlight areas of colocalisation

preclude the possibility of the incorporation of a tag affecting the normal cellular localisation of EAP45, we transfected full length (FL) SNAP-EAP45 into HeLa cells and examined its cellular localisation and its recruitment during cytokinesis, two of the well-characterised activities in which ESCRT proteins are involved.^{35,36} EAP45 largely shows a cytosolic distribution and colocalises with RAB7 (Figure 1B), a late endosome marker, consistent with previous observations.³² We were cognizant that overexpression of EAP45 might affect endosome morphology but direct calculations of this did not reveal any concerning changes (Figure S1). For visualisation of cytokinesis, a HeLa cell line constitutively expressing YFP-TSG101 was used as a control.³⁵ We observed that TSG101 was recruited to the intercellular bridge as expected (Figure 1C upper panels). Following substrate

staining and specificity verification for the SNAP tag (Figure S2), we also observed that EAP45 was recruited to a similar location (Figure 1C lower panels). The labelling method is specific, as the cells which were nontransfected showed no signal from the staining. These data show that the normal cellular distribution of EAP45 is not affected by the insertion of an N-terminal SNAP tag.

2.2 | SNAP-EAP45 rescues HIV budding in HAP1-EAP45 KO cells

We then verified the rescue functions of the expressor in HIV budding using a similar procedure to that which we reported previously.²⁹

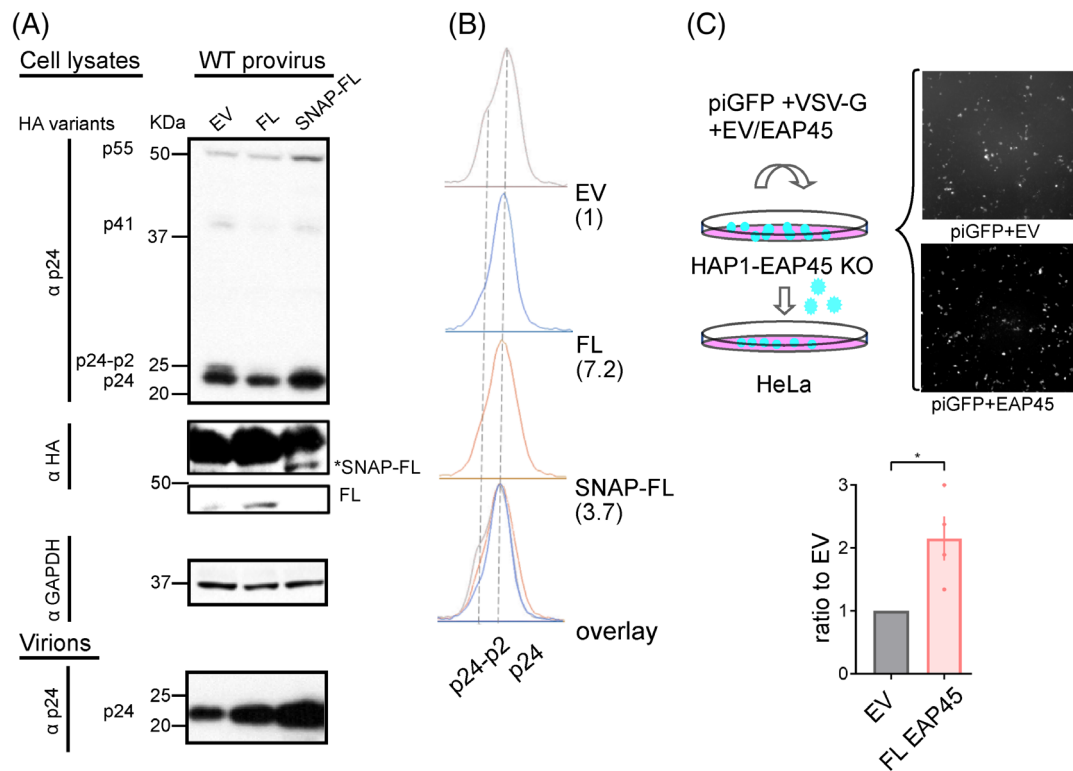


FIGURE 2 Verification of the SNAP-tag and GFP-Gag in HIV budding in HAP1 EAP45 KO cells. A, The WT provirus was co-transfected with either empty vector (EV), untagged EAP45, or SNAP-FL EAP45 in HAP1 EAP45 KO cells. Cells were lysed 2 days post transfection and supernatants were harvested for virus purification before western blotting using anti-p24 or anti-HA antibody. GAPDH is also immunoblotted as a control. Asterisk shows the band of interest. Protein size markers are indicated by the blot on the left and the densitometric analyses of the final step of Gag cleavage (p24/p24-p2; ratio in brackets) are shown next to the blots in B. C, piGFP was co-transfected with EAP45 or EV in HAP1 EAP45 KO cells with fluorescence images taken 2 days post transfection. The supernatants from the cells were collected and used for transduction onto a layer of HeLa cells for counting GFP positive cells. The number of GFP positive cells was normalised to that of the EV control. The statistical analysis was carried out using a one-sample t test on ≥ 3 replicates from two experiments

Transient expression of SNAP-FL EAP45 with WT provirus into the HAP1-EAP45 KO cells shows rescue of the virus budding defect (Figure 2A). This was accompanied by restoration of a normal rate of cleavage at the last step of Gag polyprotein processing (p24/p2), consistent with the effect observed with the non-tagged EAP45 (Figure 2B).³⁰ This suggests that fusion of a SNAP tag does not affect the function of EAP45 in rescuing HIV budding from HAP1-EAP45 KO cells. The identical phenotype of rescue/failure with the SNAP tagged ΔG and $\Delta G\Delta H$ mutants respectively was seen as was the case in our previous work with untagged versions (Figure S3). To fluorescently label Gag for imaging, we used a piGFP construct in which a GFP tag was inserted between MA and CA of the Gag polyprotein, and has previously been shown to produce GFP-Gag intracellularly.³⁷ To verify this construct in HAP1 EAP45 KO cells, we co-transfected KO cells with piGFP plasmid, VSV-G envelope, and FL EAP45 expressors. Two days post transfection the supernatants were harvested and used to transduce HeLa cells, and then GFP positive cells were counted (Figure 2C). Our data show a comparable level of GFP expression in both EV and EAP45 transfected HAP1 EAP45 KO cells, consistent with the previous observation that the effect on expressing EAP45 *in trans* is not related to

alterations in intracellular viral gene expression, which we and others have noted in previous work.^{30,38} However, when the virions were used to transduce HeLa cells, a significantly increased transduction level was observed in EAP45-expressing HAP1 cells in comparison to that of the empty vector (EV, $P = .0467$). These data confirm that the GFP labelled virus is rescued comparably with the wild-type untagged viruses in HAP1 EAP45 KO cells. Whilst it is feasible that this rescue is because of, or contributed to by events at other stages of viral export rather than the late stages of viral assembly as we postulate, these results are coherent with other data in this and in our previous published work that budding is a significant stage at which EAP45 is functioning.

2.3 | Spatial co-occurrence analysis using widefield TIRF microscopy

After verifying the specificity of the SNAP label for EAP45 and the GFP label for Gag, we devised an imaging and analysis procedure to observe and measure the co-occurrence of EAP45 and Gag at the plasma membrane using widefield TIRF microscopy, as illustrated in

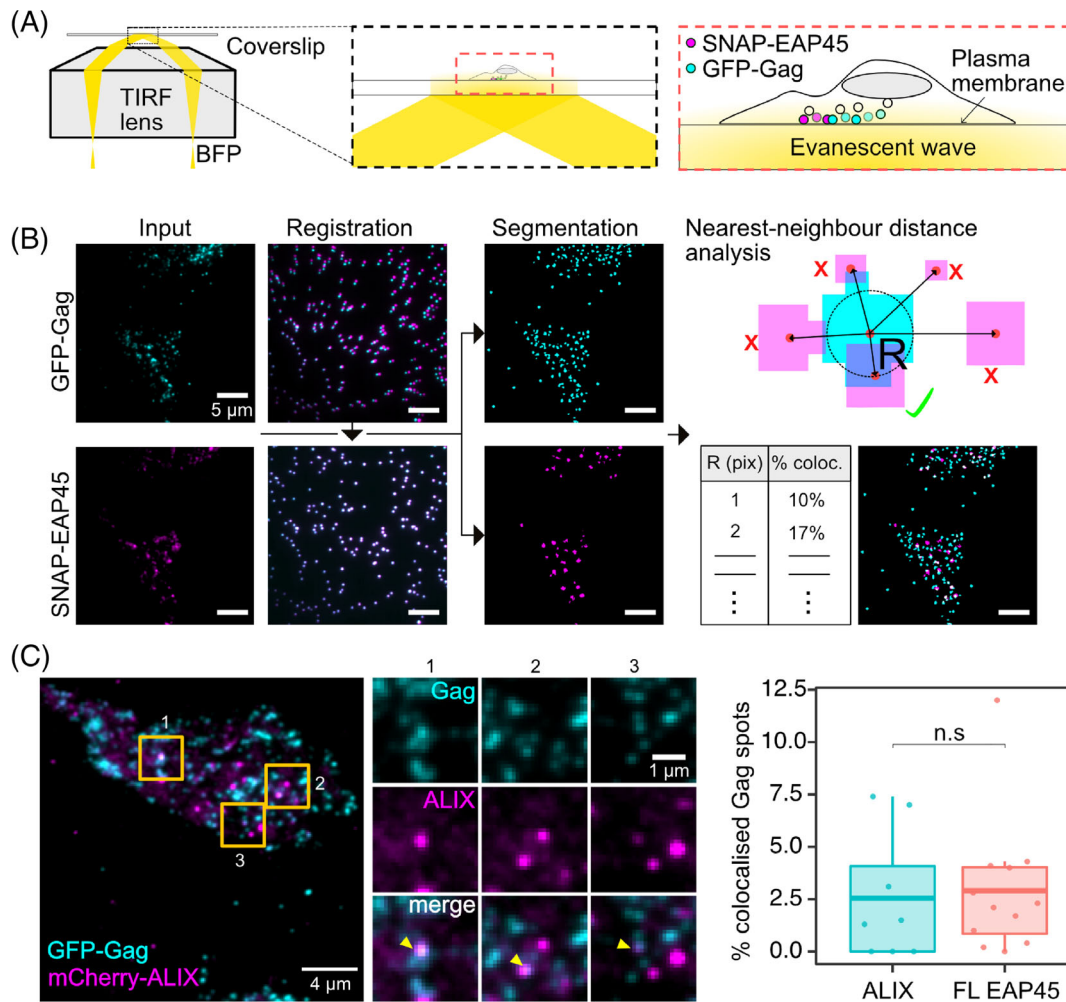


FIGURE 3 Imaging Gag and EAP45 at the plasma membrane using TIRF microscopy. A, Schematic diagram of the illumination set up used to visualise the spatial proximity of GFP-Gag clusters and EAP45 clusters in mammalian cells. B, Raw dual-colour images captured with the TIRF microscope are registered using calibration images from multicolour fluorescent beads and then segmented using the Trainable Weka Segmentation³⁹ plugin in ImageJ/Fiji.⁴⁰ A nearest-neighbour distance analysis was implemented in Matlab to quantify the spatial proximity of Gag and EAP45 or other protein of interest. Puncta found within one pixel (~ 117 nm) from a punctum in the opposite channel were labelled as ‘colocalised’. C, Co-localisation analysis applied to cells expressing ALIX and Gag, as well as cells with SNAP-FL EAP45 and Gag (the same FL EAP45 values in Figure 4E for direct comparison). Representative images of the mCherry-ALIX cells with GFP-Gag are shown, along with insets showing instances of colocalisation between the two markers. Yellow arrowheads in the insets, shown throughout this study, highlight puncta in both channels which show visible colocalisation. The plot shows the percentage of colocalised Gag puncta. Each data point represents a cell ($n = 8$ cells for ALIX, and $n = 12$ cells for FL EAP45) processed with the pipeline illustrated in, B. Welch’s two sample t test was used to compare the colocalisation results from ALIX and Gag, to those of FL EAP45 and Gag

Figure 3A. To validate this procedure, we used a nearest-neighbour distance analysis^{41,42} to search for the maximal co-occurrence from two different fluorescent labels on the same species. HeLa cells were transfected with piGFP, followed by staining with an anti-GFP nanobody conjugated with AlexaFluor647 dye. The two different fluorescent markers were expected to perfectly overlap in space, allowing us to test the maximal experimentally attainable colocalisation (Figure S4A). Images were segmented to detect puncta in both colour channels, and the centre-to-centre distances between Gag and nanobody puncta were calculated (Figure 3B). Any Gag puncta found to have a neighbouring nanobody within a given search radius were labelled as ‘colocalised’. To account for different densities of Gag

puncta per cell, the number of colocalised puncta was expressed as a percentage of the total number of detected puncta. A search radius of up to 3 pixels (350 nm) was used, and the percentage of colocalised Gag puncta was plotted as a function of this radius (Figure S4B). The percentage of colocalised puncta within 1 pixel was $\sim 75\%$, increasing to $\sim 90\%$ within 2 and 3 pixels. These percentages of colocalisation provide an estimated upper boundary for the maximum proximity expected for a sample in which a marker of interest directly binds to Gag puncta.

Following validation using this ideal sample, we examined the co-occurrence of Gag and ALIX (Figure 3C). ALIX is well known to be transiently recruited to the budding site by Gag during viral egress for

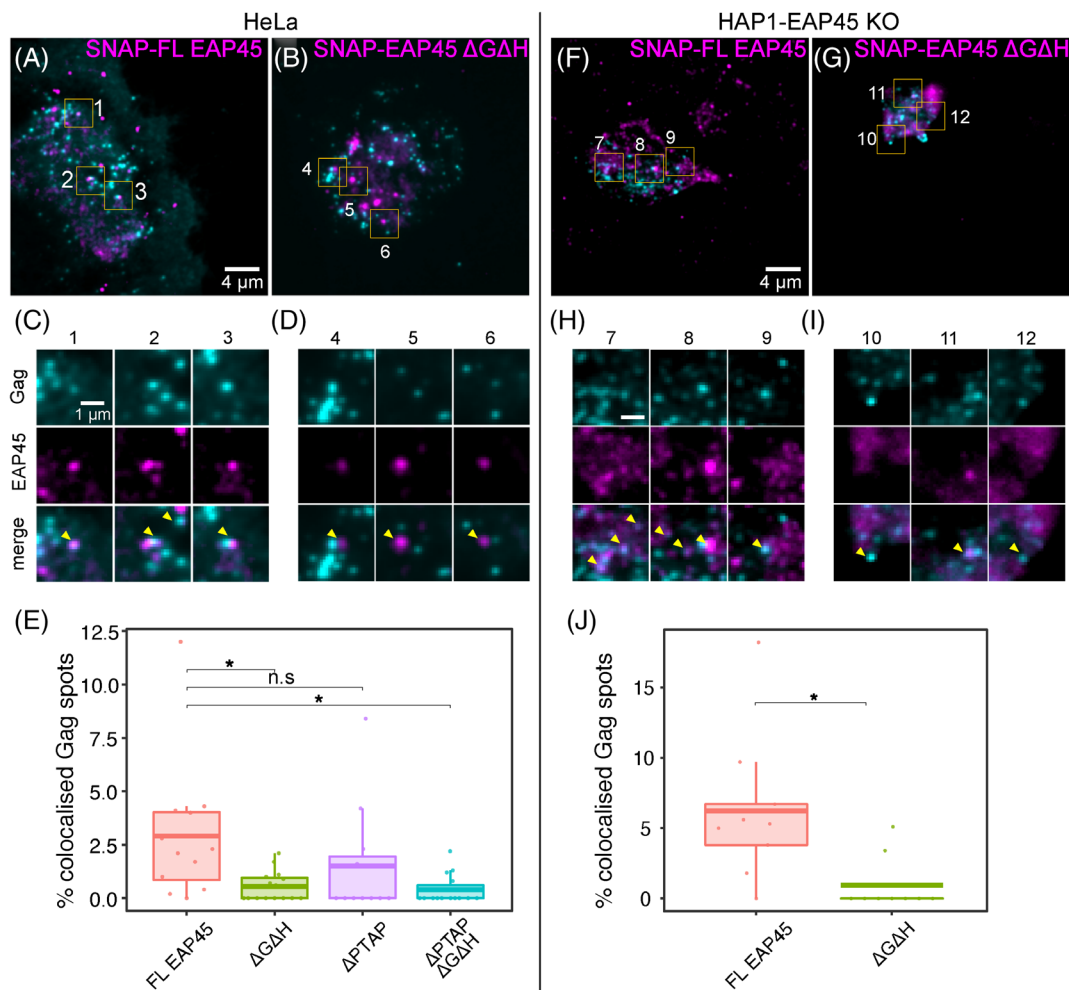


FIGURE 4 Widefield TIRF microscopy images of fixed HeLa and HAP1-EAP45KO cells with fluorescent markers for Gag and EAP45. A, Representative images for HeLa cells expressing SNAP-FL EAP45 with insets showing regions of high spatial overlap between the two markers, C, and SNAP- Δ G Δ H EAP45, B, with insets showing regions with little spatial overlap between markers, D. E, Comparison of the percentage of colocalised Gag puncta, that is, those which have an EAP45 punctum within 1 pixel, between FL EAP45 ($n = 12$), Δ G Δ H ($n = 15$), Δ PTAP ($n = 11$), and Δ PTAP- Δ G Δ H ($n = 14$) expressing HeLa cells using a One-Way ANOVA with Dunnett comparisons. F, Representative images for HAP1-EAP45KO cells expressing SNAP-FL EAP45 with insets showing regions of high spatial overlap between the two markers, H, and SNAP- Δ G Δ H EAP45, G, with insets showing regions with little spatial overlap between markers, I. J, Comparison of the percentage of colocalised Gag puncta between the FL EAP45 ($n = 9$) and Δ G Δ H EAP45 ($n = 9$) expressing HAP1-EAP45KO cells using Welch's t test

subsequent recruitment of other ESCRT components.^{14,17} We transfected piGFP into an mCherry-ALIX expressing HeLa cell line.³⁵ One day post-transfection, the cells were fixed and examined using TIRF microscopy. The nearest-neighbour analysis procedure described above (Figure 3B) was applied to search for ALIX puncta in the vicinity of Gag puncta. Based on the average size of clusters of ESCRT proteins (~ 150 nm),¹⁵ the diameter of HIV budding virions (~ 120 nm),⁴³ and the diffraction-limited resolution of our microscope (2 pixels = 234 nm), we selected a 1-pixel perimeter as a constraint for defining colocalisation between the two clusters. Our data show that around 2.5% of ALIX puncta colocalised with at least one Gag punctum within a 1-pixel distance (Figure 3C). This colocalisation rate is similar to the $\sim 1\%$ to 4% reported previously for various ESCRT components.¹⁸

2.4 | TIRF microscopy shows high spatial proximity between EAP45 and Gag compared to functionally compromised mutants

Having validated our imaging and co-occurrence analysis procedure, we imaged HeLa cells transfected with piGFP and SNAP-EAP45 followed by staining with an AlexaFluor647-conjugated SNAP substrate (Figure 4A-E). The cells were fixed at 1 day post transfection before imaging. We observed both EAP45 and Gag puncta at the plasma membrane, showing that EAP45 trafficks to the plasma membrane. This is consistent with the observation made using quantitative EM analysis showing that components of ESCRTs are located at the plasma membrane.⁴⁴ The nearest-neighbour distance analysis was applied between FL EAP45 and Gag ($n = 12$ cells, Figure 4A,C,E) and

compared to that of ALIX and Gag (Figure 3C). We observed around 3% of EAP45 molecules colocalised with Gag within our 1-pixel threshold similar to the colocalisation rate observed between ALIX and Gag (Figure 3C), suggesting that in HeLa cells both EAP45 and ALIX are recruited to the budding sites close to the plasma membrane at a similar abundance. The Glue/HO deletion mutant ($\Delta G\Delta H$) is deficient at rescuing the HIV budding defect in EAP45 KO cells, as the HO linker region responsible for this rescue by binding ESCRT-I is absent.³⁰ As expected, removal of the Glue and HO domains results in lower spatial proximity between EAP45 and Gag puncta within a diffraction-limited region than that measured for the FL EAP45 ($n = 15$ cells, Figure 4B,D,E, $P = .026$ between FL EAP45 and $\Delta G\Delta H$), reinforcing the notion that this region plays a pivotal role in linking with Gag. The PTAP domain of Gag p6 is involved in recruiting

TSG101 and thus cascading the recruitment of ESCRT-II and ESCRT-III in HIV budding.^{45,46} We hypothesised that the removal of the PTAP late domain ($\Delta PTAP$) would impair the colocalisation between EAP45 and Gag. Our data however show that even though there is a decrease in the measured colocalisation between FL EAP45 with PTAP mutants ($n = 11$ cells), this is not significantly different from that of WT Gag and FL EAP45 (Figure 4E, $P = .36$), indicating that EAP45 also co-occurs with Gag independently of PTAP. Consistently, this colocalisation with the PTAP mutant relies on an intact Glue and HO linker region, as the removal of this region completely abrogates this phenomenon ($n = 14$ cells, Figure 4E, $P = .018$ between FL EAP45 and $\Delta PTAP-\Delta G\Delta H$).

To further confirm the specificity of the colocalisation observed between EAP45 and Gag, we also examined them in HAP1-EAP45

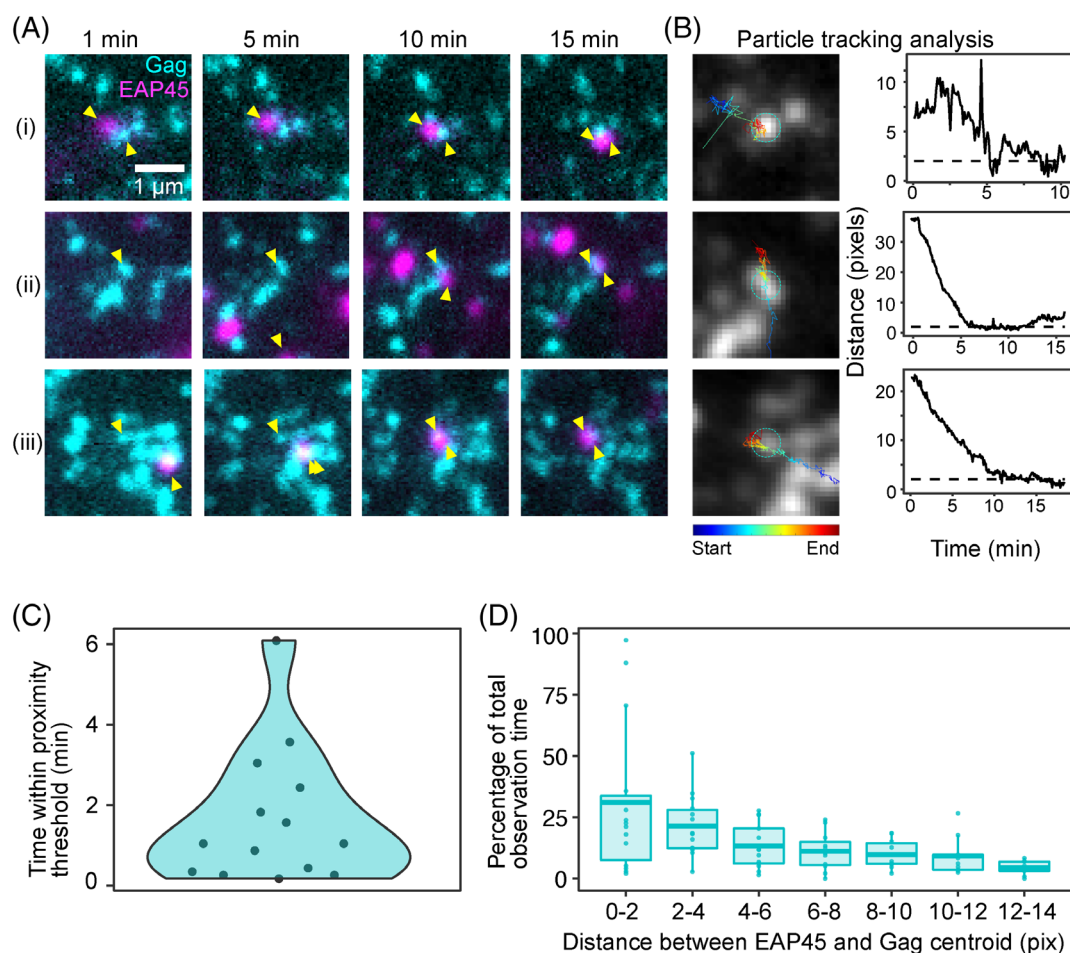


FIGURE 5 Single particle tracking on live-cell TIRF microscopy images shows a transient co-localisation between EAP45 and Gag spots from 20 seconds to several minutes. The panels in, A, show two-colour images at 1, 5, 10, and 15 minutes for different regions of interest in the live acquisitions, with the GFP-Gag channel in cyan and the SNAP-FL EAP45 channel in magenta. Yellow arrowheads are used to point out the virus and EAP45 spots which were selected for single particle tracking. The panels in, B, show the results from the co-moving frame analysis. The first column under ‘Particle tracking analysis’ shows an average grey-scale image of the stabilised Gag channel with the selected Gag punctum always in the centre of the frame and a super-imposed line plot of the path traced by the EAP45 punctum colour-coded for time. The second column under ‘Particle tracking analysis’ shows line plots of the distance in pixels between the centroids of the Gag and EAP45 puncta vs time for each of the three regions of interest in, A. The dotted line represents the colocalisation threshold, C, Kernel density plot showing the maximum consecutive colocalisation time between Gag and EAP45 over 14 regions of interest (ROIs), D, Percentage of total observation time as a function of the distance between centroids of Gag and EAP45, plotted over 2-pixel increments ($n = 14$)

KO cells, with subsequent supplementation *in trans* with FL EAP45, followed by image acquisition and analysis (Figure 4G-L). We tested the proximity of Gag and FL EAP45 ($n = 8$ cells) vs that of Gag and Δ G Δ H EAP45 ($n = 9$ cells). Our data show a significantly higher ($P = .018$) number of EAP45 puncta within the colocalisation threshold of Gag for FL (mean $\sim 6\%$) than for the Δ G Δ H mutant (mean $\sim 1\%$), as illustrated in Figure 4J, reinforcing the notion that the N terminus of EAP45 is required for the colocalisation of EAP45 and Gag by potentially providing a bridge linking EAP45 to ESCRT-I.³⁰ The findings from the nearest-neighbour analysis in both HAP1 EAP45 KO and HeLa cells are consistent with the evidence obtained biochemically showing the N terminus encompassing the H0 linker region in EAP45 plays an important role in HIV budding.

2.5 | Single particle tracking in live HeLa cells shows transient colocalisation of Gag and EAP45

The assembly of Gag particles at the cell membrane during HIV budding has been reported to occur within a time frame of ~ 10 minutes,^{11,47} and the dynamics of ESCRT protein recruitment by Gag particles have been reported for TSG101,^{11,16} VPS4A,^{5,12,15,17} some CHMP proteins of ESCRT-III^{5,11} and ALIX,^{14,17} with an association time at the membrane for different components varying from as little as a few seconds up to 20 minutes. To further validate the observed association between Gag and EAP45, and to analyse its dynamics, we used TIRF microscopy in live HeLa cells to visualise the spatiotemporal relationship between GFP-Gag and SNAP-FL EAP45 at the plasma membrane.

The HeLa cells were transfected with GFP-Gag and Gag expressors at a 1:5 ratio, similarly to previous reports,^{14,15} with SNAP-FL EAP45. The substrate for SNAP-EAP45 was added at >10 hours post-transfection when the Gag puncta are predominantly detectable at the plasma membrane.³⁷ We analysed 20-minute long live cell movies using single particle tracking. A sub-pixel fitting routine to calculate the centre position of the puncta was applied in which the distance between the centres of an EAP45 punctum and a Gag punctum were plotted over time. In the live cell movies, both Gag and EAP45 clusters move simultaneously, making it difficult to see how their relative positions are correlated over time. To visualise the relative motion of the puncta more clearly, we developed an algorithm that tracked the position of a Gag punctum and repositioned the field of view such that the detected punctum remained in the centre of the image from frame to frame. We used the Gag position as a reference point against which the motion of the EAP45 could be measured. We call this algorithm a 'co-moving frame analysis', and its steps are summarised in Figure S5. For each region of interest (ROI) extracted, the distance between the Gag and EAP45 tracks was plotted as a function of time. The puncta were considered to be 'colocalised' if the distance between their centre positions was within our previously defined 1-pixel perimeter. Our analysis shows a transient colocalisation between Gag and EAP45 puncta over a time scale of 1 to 5 minutes, with a mean consecutive colocalisation time of ~ 1.7 minutes

(Figure 5C). This is consistent with the time frame of colocalisation reported for other ESCRT proteins. Within 14 analysed ROIs, there appear to be three classes of potential movements between EAP45 and Gag (Figure S6): (1) EAP45 colocalises with Gag multiple times (Figure 5A,B [i]—Video S1; 7 out of 14 events); (2) EAP45 approaches Gag and remains colocalised with Gag for a span of time before leaving again (Figure 5A,B [ii]—Video S2; 4 out of 14 events); (3) EAP45 approaches Gag and remains colocalised with Gag during the time of the recording (Figure 5A,B [iii]—Video S3; 3 out of 14 events). Furthermore, for all ROIs analysed, EAP45 puncta spent $\sim 30\%$ of the total observation time within the threshold distance from a Gag particle (Figure 5D). The distance vs time traces and the overlaid tracks in Figure 5B suggest that the EAP45 puncta remain stationary or linger in the vicinity of the Gag particle. This indicates a possible transient interaction between Gag and EAP45, similar to that of Gag and other ESCRT components during viral egress.

2.6 | The Glue domain is not required for the localisation of EAP45 at the late endosome but is required for recruitment to the midbody

ESCRT-II components are also involved in MVB formation and cytokinesis.^{25,48-50} It has been hypothesised the Glue domain plays an important role in those activities. However, the exact domain requirements of EAP45 in metazoans remain ill-defined. We used the specific labelling from the SNAP tag to investigate this in more detail. Unexpectedly, EAP45 localises to late endosomes despite removal of the Glue domain (Δ G) (Figure S7, suggesting that the Glue domain, which has binding sites for both ubiquitin and lipids,³² is not necessary for the recruitment of EAP45 to late endosomes. Further deletion of the H0 linker region (Δ G Δ H) greatly reduces the observed colocalisation, suggesting the H0 linker region rather than the Glue domain on its own is crucial in anchoring EAP45 at late endosomes. The H0 linker region is required for binding to subunits of ESCRT-I *in vitro*,^{22,23} therefore it is possible that ESCRT-I colocalises with and recruits EAP45 at late endosomes. We used a HeLa YFP-TSG101 cell line to examine this possibility. Upon transfection of SNAP-FL EAP45 expressor, we observed a significant cytosolic colocalisation of EAP45 with TSG101 at late endosomes (Figure 6A). This colocalisation is also observed in the Δ G mutant but not in the Δ G Δ H mutant, which would be consistent with a role for ESCRT-I in the recruitment of ESCRT-II to late endosomes and that this recruitment depends on an intact H0 linker region.

In addition to its role in endosomal membrane anchoring, EAP45 is recruited to the intercellular bridge during cytokinesis (Figure 1C).⁵⁰ To better understand which domains in EAP45 are required for this, we transfected expressors of EAP45 and the derived mutants into HeLa cells and imaged the cellular distribution of EAP45 at the intercellular bridge during cytokinesis (Figure 6B-D). Full length EAP45 is recruited to the intercellular bridge as expected, but this colocalisation is significantly decreased when the Glue domain (Δ G) is removed, suggesting the Glue domain is important for efficient recruitment in

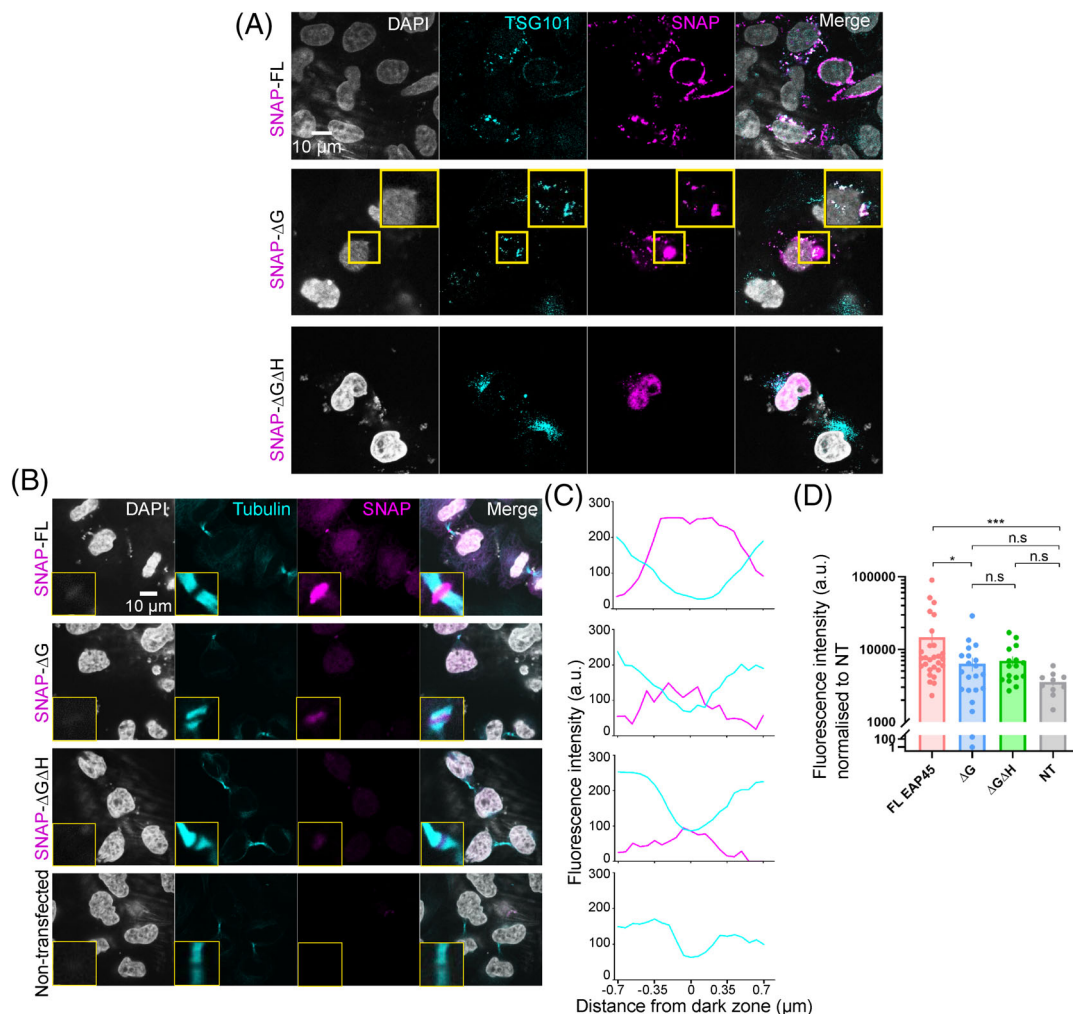


FIGURE 6 Glue domain is not required for the localisation of EAP45 at the late endosome, but it is required for its localisation at the intercellular bridge during cytokinesis. Confocal images of YFP-TSG101 HeLa cells, A, transfected with different SNAP-EAP45 constructs and stained 1 day post-transfection with DAPI for nuclei and AlexaFluor647 conjugated SNAP substrates for EAP45. B, Confocal images of HeLa cells stained with DAPI, α -tubulin, and AlexaFluor647-SNAP substrates for EAP45. C, Plots of line density profiles across the intercellular bridge for each condition shown in, B. D, Quantification of the intensities for each condition where EAP45 is recruited at the intercellular bridge is shown. The statistical analysis was carried out using a Kruskal-Wallis test ($n = 28, 21, 16, 10$ for FL EAP45, ΔG , $\Delta G\Delta H$ and NT, respectively, from two independent experiments). Error bars represent the SEM

cytokinesis in contrast to the findings in late endosomes. Further removal of the H0 linker region ($\Delta G\Delta H$) does not significantly decrease recruitment further, stressing the importance of the Glue domain in cytokinesis and indicating that the two mutants may traffic equivalently within the cell.

3 | DISCUSSION

The requirement for and potential roles of ESCRT-II in MVB formation, cytokinesis, and HIV budding have all been areas of controversy, with some reports suggesting it is redundant.^{22,35,36} More recent data in cytokinesis^{48,50} and HIV budding^{29,30} appear to revise this view and strongly implicate ESCRT-II in a bridging role between ESCRT-I and ESCRT-III as was originally reported for endosomal cargo

sorting.^{20,27,31} Our previous data showed that expressing EAP45 *in trans* can rescue an HIV budding defect in EAP45 KO cells and our subsequent biochemical analysis pinpointed the H0 linker domain in EAP45 as crucial for this function.³⁰ Here, using TIRF microscopy we now expand these findings and confirm them visually.

We observed EAP45 expressed in close proximity to, or at, the plasma membrane, similarly to other ESCRT members documented previously.⁴⁴ Colocalisation is not extensively observed (around 1%–6%) between ALIX and Gag (Figure 3C) and EAP45 and Gag (Figure 4E,J) but these rates are consistent with those reported by others using dSTORM to measure both endogenously and exogenously expressed ESCRT components with Gag (1.5%–3.4%).¹⁸ Given the maximum experimentally attainable colocalisation measured using the AlexaFluor647 nanobody targeting GFP (Figure S4), this number is an underestimate of the total events by a factor of 25%. The

infrequent static colocalisation seen has been observed previously¹⁸ and is likely attributable at least to the documented transient nature of recruitment of ESCRT proteins.

We show that in HAP1 EAP45 KO cells there is a higher colocalisation rate between SNAP-FL EAP45 and Gag than in HeLa cells (Figure 4). This reflects the fact that in the latter endogenously produced EAP45 will contribute to a functional pool and affirms that EAP45 is being actively recruited *in trans* to viral budding sites. Interestingly colocalisation of EAP45 and Gag is not uniquely dependent on the canonical 'late domain' recruiting motif PTAP in the viral protein, because of deletion of this motif (Δ PTAP Gag) does not reduce colocalisation by a statistically significantly amount (Figure 4E). Given that the level of recruitment and dynamics at the plasma membrane between WT and Δ PTAP Gag are similar,^{11,12,51} this could be explained by an alternative route of recruitment of EAP45 for example by ALIX via its interaction with TSG101 of ESCRT-I.^{8,52}

Our analysis of the colocalisation of EAP45 and Gag is consistent with a model in which EAP45 is actively recruited and indicates that the N terminal region of EAP45 is crucial for its association with Gag at the plasma membrane. This is consistent with our previous biochemical evidence wherein deletion of the Glue and H0 regions completely abolished the rescue of HIV-1 budding by exogenous EAP45 in the EAP45 KO cells.³⁰ This domain dependence of the functional interaction is also

important in aiding the recruitment of ESCRT-II at the endosomal membrane (Figure 1B and Figure S7). However, it is less important in the context of ubiquitin and lipid binding mirroring previous reports on the recruitment of ESCRT-II at the endosomal membrane in yeast in which H0 mediated anchoring appears more critical than the Glue domain integrity.²⁵ When we compared these observations to the situation in cytokinesis (Figure 6B-D) by contrast the Glue domain appeared to be more critical possibly by interaction with the unique local lipid components.⁵³ Further analysis beyond the scope of this paper would be needed to analyse this in detail.

Our live imaging experiments reveal dynamic recruitment of EAP45 to the Gag assembling sites (Figure 5 and Figure S6). On average, EAP45 colocalises with Gag puncta for a period of 1.7 minutes. Remarkably, for 30% of the total recording time (~5 minutes) EAP45 colocalises with Gag. We observed three distinct classes of movement of EAP45. In some cases the recruitment resembled that of CHMP4B/VPS4 which are recruited multiple times until scission happens^{5,17}; in others the pattern is one of more prolonged tenure at the site similar to that of TSG101 which, once recruited, remains at the site and could serve as an adaptor for the further recruitment of downstream components.^{15,16} Third, a small but consistent population of EAP45 molecules appear to stay permanently with Gag once recruited (Figure 7). This is very likely attributable to molecules being

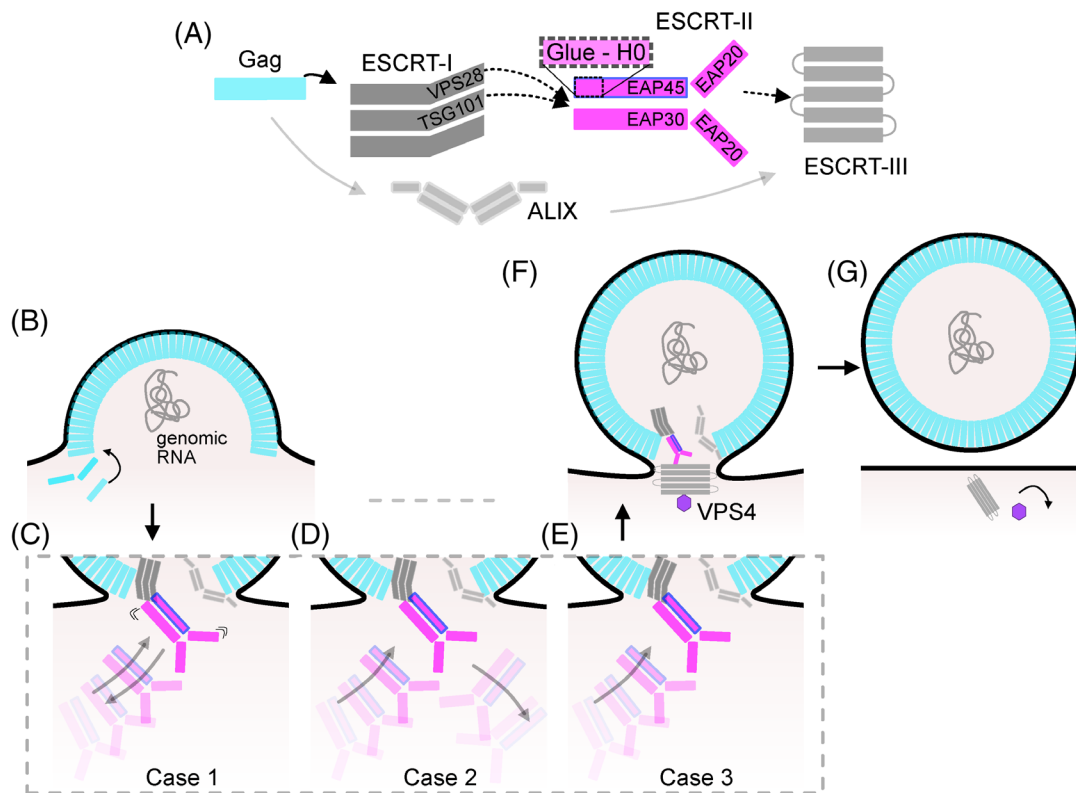


FIGURE 7 Proposed models for the role of ESCRT-II in HIV budding. A, Cartoon showing the current understanding of the ESCRT protein apparatus in HIV budding. The ESCRT-II complex is shown enlarged, with the EAP45 protein highlighted in purple, and the Glue-H0 region surrounded by dotted lines. B, HIV Gag accumulation causes deformation of the plasma membrane, leading to the recruitment of ESCRTs. Three possible models of ESCRT-II recruitment are illustrated: C, recruitment in which the ESCRT-II oscillates towards and away from the bud, D, transient recruitment followed by decoupling, and E, persistent recruitment. F, shows the final stage before membrane scission in which the polymerised ESCRT-III is recruited to the budding neck and acts in combination with VPS4 to achieve membrane scission and bud egress, G

packaged within the virions in a similar fashion to that observed with ALIX and TSG101.^{14,54} However, some degree of non-specific aggregation is difficult to exclude completely. Because of ESCRT recruitment events were transient, our experiments were limited to time windows during which Gag puncta emerge to maximise capture of co-occurrence events. Future work with a fully automated TIRF microscope for long-term time-lapse imaging of the plasma membrane would be useful to include longer time windows and more frequent observations to more completely capture the Gag/EAP45 recruitment. Distinguishing the details of the individual recruitment patterns and their functional role would require more in-depth analysis and might lead to the identification of more than one functional role for EAP45 in HIV export.

Our findings add to the growing body of evidence confirming that ESCRT-II is a significant and important component of the HIV-1 budding process. The patterns of recruitment of EAP45 provide intriguing hints that there may be more than one functional role for this protein in this process. The contrast between the critical functional domains of EAP45 in the budding and cytokinesis pathways also point towards possible therapeutic interventions that might be weighted towards affecting the virus whilst leaving host cell functions less perturbed.

4 | MATERIALS AND METHODS

4.1 | Plasmids and cells

All cells used in this study were grown in DMEM with 10% FCS at 37°C in 5% CO₂ incubator. HeLa YFP-TSG101 and mCherry-ALIX cells were gifts from Juan Martin-Serrano at KCL. pBH10ΔBgIII-WT and pCMV-VSV-G, pEF-EAP45-HA were reported previously.²⁹ piGFP was a gift from Benjamin Chen at Mount Sinai and was described previously.³⁷ A sole Gag expressor (HVPgagpro-) was also described previously.⁵⁵ SNAP-FL-EAP45, SNAP-ΔG-EAP45 and SNAP-ΔGΔH-EAP45 were constructed by VectorBuilder. The pBH10Gag-GFP-PTAP mutant was cloned by ligating the BssIII and SpeI digested fragments from the piGFP vector to the same sites in pBH10Gag-PTAP, which had been rendered Gag/pol deficient by creating a deletion between BclI and Ball sites.

4.2 | Transfection

For transfection, the HeLa cells were transfected with Fugene HD (Promega) and HAP-EAP45 KO cells were transfected with Turbofectin (OriGene). Both the SNAP-expressor rescue experiment and the transfection of piGFP in HAP1-EAP45 KO cells were done similarly as described before.³⁰ Briefly, 150 ng of pBH10ΔBgIII-WT or 250 ng of piGFP was co-transfected with 45 ng of SNAP-FL-EAP45 or pEF-EAP45-HA, together with pCMV-VSV-G, respectively, in a well of a 24 well plate. The supernatant was harvested for virion

purification and cells were lysed for immunoblotting at 2 days post transfection.

8-well glass-bottom Lab-Tek slides were used in both fixed and live cell imaging. For fixed cell imaging, HeLa cells were co-transfected with 100 ng piGFP and 60 ng of SNAP-FL-EAP45. HeLa-mCherry-ALIX cells were transfected with 100 ng piGFP. HAP1-EAP45 KO cells were co-transfected with 200 ng piGFP and 72 ng of SNAP-FL-EAP45. At 24 hours post transfection, the cells were fixed, permeabilised with Trion X-100 and stained with the SNAP-Surface AlexaFluor647 (NEB) at 4 μM for 1 hour. For live cell experiments, a total amount of 120 ng of piGFP and HVPgagpro- plasmids at a ratio of 1:5 were co-transfected with 72 ng of SNAP-FL-EAP45. At >10 hours post transfection, the cells were stained with cell permeable live SiR-SNAP (NEB) at 3 μM for 30 minutes followed by washes according to the manufacturer's instructions before examination by widefield TIRF microscopy.

4.3 | Immunoblotting

Immunoblotting was done essentially as reported previously.³⁰ Briefly, at 2 days post transfection, supernatants were harvested for virion purification and monolayers were lysed in cell culture lysis buffer (CCLR, Promega) for immunoblotting. The primary antibodies used in this study were anti-p24 (NIBSC), anti-GAPDH (Abcam), anti-HA (ThermoFisher), and secondary antibodies used were goat anti-mouse IgG-HRP (Cell Signalling Technology) and goat anti-rabbit IgG-HRP (ThermoFisher). Densitometric analysis of the target bands was done in ImageJ⁴⁰(NIH) with traces of p24 and p24-p2 highlighted to show the differences in the final cleavage product.

4.4 | Confocal microscopy

HeLa or HeLa-TSG101-GFP cells were seeded into 8-well slides (EZ slides, Merck). At 24-hour post seeding, the cells were transfected with 100 ng of either SNAP-FL, SNAP-ΔG, or SNAP-ΔGΔH-EAP45 expressor. This was followed by fixation with paraformaldehyde and permeabilisation with Triton X-100 and staining with SNAP-Surface AlexaFluor647 (NEB) at 4 μM concentration for SNAP-EAP45 according to the manufacturer's instructions and DAPI for nuclei on the following day. A primary antibody to RAB7 (Abcam) or anti-Tubulin (Sigma) was also added on some occasions followed by staining with the secondary antibody conjugated with either AlexaFluor488 or AlexaFluor647 (ThermoFisher) before imaging using Leica SP5 confocal fluorescence microscope. The fluorescence intensity was calculated within the dark zone during cytokinesis for the SNAP channel. The normalised fluorescence intensity was obtained by subtracting the fluorescence intensity from the averaged non-transfected (NT) cells for each experiment. Negative values were obtained for those where the fluorescence intensities are smaller than the averaged background from NT. To compensate these, a constant

value was used to transform all the data points before statistical analyses were carried out.

4.5 | Widefield TIRF fixed cell imaging

Fixed cell images using widefield TIRF microscopy were acquired with a custom-built microscope based on an Olympus (Center Valley, PA) IX-73 frame with a 488-nm laser (Coherent Sapphire 488-300 CW CDRH), a 561-nm laser (Cobolt Jive 500 561 nm), and a 647-nm laser (MPB Communications Inc. VFL-P-300-647-OEM1-B1). Laser light entering the microscope frame was reflected from a dichroic mirror (Chroma ZT488/561/647rpc) into a 100× 1.49 NA oil objective lens (Olympus UAPON100XOTIRF), and then onto the sample. Light emitted by the sample passed through the dichroic and a set of 25 mm band-pass filters (Semrock FF01-525/45-25, Semrock FF01-600/37-25, and Semrock FF01-680/42-25 respectively for the 488, 561, and 647-nm laser lines) before reaching the microscope side port. Images were then relayed onto two cameras (Andor iXon Ultra 897) by a 1.3× magnification Cairn Twincam image splitter with a dichroic beam splitter (T565spxr-UF3) which allows imaging of emitted wavelengths between 390 and 555 nm in the transmission port and 575-1000 nm in the reflection port. The pixel size in the sample plane was measured to be 117 nm.

4.6 | Nearest-neighbour distance analysis of fixed cell images

We used an object-based nearest-neighbour analysis method in which we segment the registered images for each colour channel, locate the centroid of the fluorescent spots, and search for puncta in the opposite colour channel within a neighbourhood of 3 pixels (~350 nm). A distance threshold within the diffraction-limited resolution of our microscope (1 pixel~117 nm) was selected to designate instances in which these molecules could be interacting, and any puncta found within this threshold from the centroid of the opposite channel were labelled as 'colocalised'. Raw dual-colour images were registered to correct for chromatic offset using the DoM plugin⁵⁶ in Fiji,⁴⁰ using 7 pixels as the maximum shift between images, a value of 15 for the SNR filter, and a PSF SD of 1 pixel. The registered images were then segmented using the Trainable Weka Segmentation plugin from Fiji/ImageJ³⁹ with the default Fast Random Forest classifier. Three classes were defined (small blobs, large blobs, and background) and images were annotated to identify single fluorescent puncta in focus (small blobs), large aggregates of puncta (large blobs), and background. The segmented images were then imported into a custom Matlab (The MathWorks, Natick) script which implemented a nearest neighbour algorithm to check, for each identified segmented spot, the distance from its nearest neighbours in the opposite colour channel. The function *natsortfiles* was used to sort the data.⁵⁷ All distances for each image were recorded and exported in a .csv file. The .csv files for all experiments were imported into an R (R Core Team, 2013) script

that was used to plot the files and run the statistical analysis on the different experimental conditions.

4.7 | Widefield TIRF live cell imaging

Live cell images using widefield TIRF microscopy were acquired with a custom-built microscope based on an Olympus (Center Valley, PA) IX-71 frame with a 488-nm laser (Toptica iBeam SMART), a 561-nm laser (Coherent OBIS LS), and a 640-nm laser (Cobolt MLD). Laser light entering the microscope frame was reflected from a dichroic mirror (Chroma ZT405/488/561/640rpc) into a 100× 1.49 NA oil objective lens (Olympus UAPON100XOTIRF), and then onto the sample. Light emitted by the sample passed through the dichroic and a set of 25 mm band-pass filters (Semrock FF01-525/45-25, Semrock FF01-600/37-25, and Semrock FF01-680/42-25 respectively for the 488, 561, and 647-nm laser lines) before reaching the microscope side port. Images were then relayed onto a sCMOS camera (Hamamatsu Orca Flash v4.0). Live cell TIRF images were acquired in two colour channels every 5 or 10 seconds with a 100 ms exposure time over 15 to 20 minutes. The pixel size at the image plane is ~50 nm (6.45 μm pixels at the camera de-magnified by the 100× objective and a 1.3× relay lens).

4.8 | Single particle tracking in live cell images

The dual-colour live cell movies were registered to correct for chromatic offset using the DoM plugin⁵⁶ in Fiji,⁴⁰ and regions of interest of ~80 × 80 pixels (~1.3 × 1.3 μm²) were manually extracted in EAP45 puncta were found in the vicinity of a Gag punctum. The Gag and the EAP45 puncta were tracked independently using TrackMate v4.0.0⁵⁸ using a radius of 4 pixels (~200 nm), a threshold value of 2 for particle detection with sub-pixel localisation, and the LAP tracker for tracking. The resulting tracks were imported into Matlab for nearest neighbour analysis.

A custom Matlab script was written to import TrackMate tracks. The distances between x,y positions of the tracks in each channel are calculated and output as a .csv file. For ease of visualisation, a new frame is generated centred around the x,y position of the Gag track such that the Gag particle is always at the centre of the frame, and the position of the EAP45 particle is shown relative to the new frame of reference. This co-moving frame analysis makes it easy to visualise the motion of two puncta over time in a 2D image. We show the average image of the immobilised Gag punctum, and the relative motion of EAP45 on top of this image, colour coded as a function of time.

4.9 | Statistical analysis

For the case in which only two experimental data sets were compared, such as in Figure 3C for ALIX and FL EAP45, and Figure 4J for FL EAP45 and ΔGΔH, Welch's two sample *t* test was used with ns:

non-significance, * for $P < .05$, ** for $P < .01$, and *** for $P < .001$. Boxplots were overlaid on the raw data points, with the bold horizontal line showing the mean, and whiskers represent the largest and smallest value within 1.5 times the interquartile range above 75th and 25th percentile, respectively. For the case in which more than two conditions were compared (Figure 4E), a One-Way ANOVA with Dunnett Comparison was used to compare the FL EAP45 condition to each of the functionally compromised mutants ($\Delta G\Delta H$, $\Delta PTAP$, $\Delta PTAP-\Delta G\Delta H$) with ns: non-significance, * for $P < .05$, ** for $P < .01$, and *** for $P < .001$. In Figure 6, error bars represent the SEM. A Kolmogorov-Smirnov test was used initially for a normality analysis showing the data are not parametrically distributed. A Kruskal-Wallis test was then used to test for statistical significance. All statistical tests were performed using R or GraphPad Prism.

4.10 | Software and data availability

The Matlab (Natick, MA) code used for the nearest-neighbour analysis for the fixed cell co-occurrence experiments, and the co-moving frame analysis for the live cell tracking experiments are available at our online repository: https://github.com/pedropabloVR/Meng_VallejoRamirez_EAP45_supportingCode. The R scripts used to generate the plots in Figures 3–5, Figures S3, S4, and S6 can also be found in this repository, along with the processed data.

ACKNOWLEDGMENTS

We would like to thank Eric J. Rees and John Sinclair for helpful discussions. We are grateful to Juan Martin-Serrano and Benjamin Chen for providing the cell lines and plasmid, respectively, used in this study. We thank Ricardo Henriques for his BioRxiv preprint LaTeX template. We also acknowledge the support from the Cambridge NIHR BRC Cell Phenotyping Hub on confocal imaging. This work is supported by the Research Visit Grant by the Microbiology Society (BM), Gates Cambridge Scholarship (PVR), UK Medical Research Council (MRC) Grant (MR/N022993/1) (JCK and AMLL), MRC Grants (MR/K015850/1 and MR/K02292X/1) (CFK), UK Engineering and Physical Sciences Research Council, EPSRC Grants (EP/L015889/1 and EP/H018301/1) (CFK), Wellcome Trust Grants (203249/Z/16/Z and 089703/Z/09/Z) (CFK), MedImmune, the RCUK under the Technology Touching Life Initiative, and Infinitus China Ltd (CFK).

CONFLICT OF INTEREST

The authors declare that they have no conflicts of interest with the contents of this article.

AUTHOR CONTRIBUTIONS

Bo Meng, conceptualization, funding acquisition, data curation, formal analysis, investigation, methodology, validation, visualisation, writing-original draft, writing-review and editing; **Pedro P. Vallejo Ramirez**, data curation, formal analysis, investigation, methodology, software, validation, visualisation, writing-original draft, writing-review and

editing; **Katharina Scherer**, data curation, investigation, writing-review and editing; **Ezra Bruggeman**, software; **Julia C. Kenyon**, conceptualization, funding acquisition, project administration, supervision, writing-review and editing; **Clemens F. Kaminski**, conceptualization, funding acquisition, project administration, resources, supervision, writing-review and editing; **Andrew M. Lever**, conceptualization, funding acquisition, project administration, resources, supervision, writing-review and editing.

PEER REVIEW

The peer review history for this article is available at <https://publons.com/publon/10.1111/tra.12820>.

ORCID

Andrew M. Lever  <https://orcid.org/0000-0001-9819-4453>

REFERENCES

- Williams RL, Urbe S. The emerging shape of the ESCRT machinery. *Nat Rev Mol Cell Biol*. 2007;8:355-368.
- Schöneberg J, Pavlin MR, Yan S, et al. ATP-dependent force generation and membrane scission by ESCRT-III and Vps4. *Science*. 2018; 362:1423-1428.
- Sundquist WI, Kräusslich HG. HIV-1 assembly, budding, and maturation. *Cold Spring Harb Perspect Med*. 2012;2:1-24.
- Meng B, Lever AM. Wrapping up the bad news: HIV assembly and release. *Retrovirology*. 2013;10:5.
- Johnson DS, Bleck M, Simon SM. Timing of ESCRT-III protein recruitment and membrane scission during HIV-1 assembly. *Elife*. 2018;7. <https://doi.org/10.7554/eLife.36221>
- Dubois L, Ronquist KG, Ek B, Ronquist G, Larsson A. Proteomic profiling of detergent resistant membranes (lipid rafts) of prostasomes. *Mol Cell Proteomics*. 2015;14:3015-3022.
- Strack B, Calistri A, Craig S, Popova E, Gottlinger HG. AIP1/ALIX is a binding partner for HIV-1 p6 and EIAV p9 functioning in virus budding. *Cell*. 2003;114:689-699.
- Von Schwedler UK, Stuchell M, Müller B, et al. The protein network of HIV budding. *Cell*. 2003;114:701-713.
- Martin-Serrano J, Bieniasz PD. A bipartite late-budding domain in human immunodeficiency virus type 1. *J Virol*. 2003;77:12373-12377.
- Demirov DG, Orenstein JM, Freed EO. The late domain of human immunodeficiency virus type 1 p6 promotes virus release in a cell type-dependent manner. *J Virol*. 2002;76:105-117.
- Jouvenet N, Zhadina M, Bieniasz PD, Simon SM. Dynamics of ESCRT protein recruitment during retroviral assembly. *Nat Cell Biol*. 2011;13: 394-401.
- Baumgartel V, Ivanchenko S, Dupont A, et al. Live-cell visualization of dynamics of HIV budding site interactions with an ESCRT component. *Nat Cell Biol*. 2011;13:469-474.
- Ivanchenko S, Godinez WJ, Lampe M, et al. Dynamics of HIV-1 assembly and release. *PLoS Pathog*. 2009;5:e1000652.
- Ku PI, Bendjennat M, Ballew J, Landesman MB, Saffarian S. ALIX is recruited temporarily into HIV-1 budding sites at the end of Gag assembly. *PLoS One*. 2014;9:e96950. <https://doi.org/10.1371/journal.pone.0096950>
- Bleck M, Itano MS, Johnson DS, et al. Temporal and spatial organization of ESCRT protein recruitment during HIV-1 budding. *Proc Natl Acad Sci U S A*. 2014;111:12211-12216. <https://doi.org/10.1073/pnas.1321655111>
- Hoffman HK, Fernandez MV, Groves NS, Freed EO, Van Engelenburg SB. Genomic tagging of endogenous human ESCRT-I

- complex preserves ESCRT-mediated membrane-remodeling functions. *J Biol Chem.* 2019;294:16266-16281. <https://doi.org/10.1074/jbc.RA119.009372>
17. Gupta S, Bendjennat M, Saffarian S. Abrogating ALIX interactions results in stuttering of the ESCRT machinery. *Viruses.* 2020;12:1032-1048. <https://doi.org/10.3390/v12091032>
 18. Prescher J, Baumgärtel V, Ivanchenko S, et al. Super-resolution imaging of ESCRT-proteins at HIV-1 assembly sites. *PLoS Pathog.* 2015; 45:613-634.
 19. Scourfield EJ, Martin-Serrano J. Growing functions of the ESCRT machinery in cell biology and viral replication. *Biochem Soc Trans.* 2017;45:613-634.
 20. Teo H, Perisic O, Gonzalez B, Williams RL. ESCRT-II, an endosome-associated complex required for protein sorting: crystal structure and interactions with ESCRT-III and membranes. *Dev Cell.* 2004;7:559-569.
 21. Gill DJ, Teo H, Sun J, et al. Structural insight into the ESCRT-I-/II link and its role in MVB trafficking. *EMBO J.* 2007;26:600-612.
 22. Langelier C, von Schwedler UK, Fisher RD, et al. Human ESCRT-II complex and its role in human immunodeficiency virus type 1 release. *J Virol.* 2006;80:9465-9480.
 23. Im YJ, Hurley JH. Integrated structural model and membrane targeting mechanism of the human ESCRT-II complex. *Dev Cell.* 2008; 14:902-913.
 24. Pineda-Molina E, Belrhali H, Piefer AJ, Akula I, Bates P, Weissenhorn W. The crystal structure of the C-terminal domain of Vps28 reveals a conserved surface required for Vps20 recruitment. *Traffic.* 2006;7:1007-1016.
 25. Mageswaran SK, Johnson NK, Odorizzi G, Babst M. Constitutively active ESCRT-II suppresses the MVB-sorting phenotype of ESCRT-0 and ESCRT-I mutants. *Mol Biol Cell.* 2015;26:554-568.
 26. Tang S, Buchkovich NJ, Henne WM, Banjade S, Kim YJ, Emr SD. ESCRT-III activation by parallel action of ESCRT-I/II and ESCRT-0/Bro1 during MVB biogenesis. *Elife.* 2016;5:1-12.
 27. Babst M, Katzmann DJ, Snyder WB, Wendland B, Emr SD. Endosome-associated complex, ESCRT-II, recruits transport machinery for protein sorting at the multivesicular body. *Dev Cell.* 2002;3:283-289.
 28. Carlson LA, Hurley JH. In vitro reconstitution of the ordered assembly of the endosomal sorting complex required for transport at membrane-bound HIV-1 Gag clusters. *Proc Natl Acad Sci U S A.* 2012; 109:16928-16933.
 29. Meng B, Ip NC, Prestwood LJ, Abbink TE, Lever AM. Evidence that the endosomal sorting complex required for transport-II (ESCRT-II) is required for efficient human immunodeficiency virus-1 (HIV-1) production. *Retrovirology.* 2015;12:72.
 30. Meng B, Ip NCY, Abbink TEM, Kenyon JC, Lever AML. ESCRT-II functions by linking to ESCRT-I in human immunodeficiency virus-1 budding. *Cell Microbiol.* 2020;22:e13161. <https://doi.org/10.1111/cmi.13161>
 31. Teo H, Gill DJ, Sun J, et al. ESCRT-I core and ESCRT-II GLUE domain structures reveal role for GLUE in linking to ESCRT-I and membranes. *Cell.* 2006;125:99-111.
 32. Slagsvold T, Aasland R, Hirano S, et al. Eap45 in mammalian ESCRT-II binds ubiquitin via a phosphoinositide-interacting GLUE domain. *J Biol Chem.* 2005;280:19600-19606.
 33. Axelrod D. Total internal reflection fluorescence microscopy in cell biology. *Traffic.* 2001;2:764-774. <https://doi.org/10.1034/j.1600-0854.2001.21104.x>
 34. Keppler A, Kindermann M, Gendreizig S, Pick H, Vogel H, Johnsson K. Labeling of fusion proteins of O6-alkylguanine-DNA alkyltransferase with small molecules in vivo and in vitro. *Methods.* 2004;32:437-444. <https://doi.org/10.1016/j.jymeth.2003.10.007>
 35. Carlton JG, Martin-Serrano J. Parallels between cytokinesis and retroviral budding: a role for the ESCRT machinery. *Science.* 2007;316:1908-1912.
 36. Morita E, Sandrin V, Chung HY, et al. Human ESCRT and ALIX proteins interact with proteins of the midbody and function in cytokinesis. *EMBO J.* 2007;26:4215-4227.
 37. Hubner W, Chen P, Portillo AD, Liu Y, Gordon RE, Chen BK. Sequence of human immunodeficiency virus type 1 (HIV-1) Gag localization and oligomerization monitored with live confocal imaging of a replication-competent, fluorescently tagged HIV-1. *J Virol.* 2007;81: 12596-12607. <https://doi.org/10.1128/jvi.01088-07>
 38. Ghoujal B, Milev MP, Ajamian L, Abel K, Mouland AJ. ESCRT-II's involvement in HIV-1 genomic RNA trafficking and assembly. *Biol Cell.* 2012;104:706-721.
 39. Arganda-Carreras I, Kaynig V, Rueden C, et al. Trainable Weka segmentation: a machine learning tool for microscopy pixel classification. *Bioinformatics.* 2017;33:2424-2426. <https://doi.org/10.1093/bioinformatics/btx180>
 40. Schindelin J, Arganda-Carreras I, Frise E, et al. Fiji: an open-source platform for biological-image analysis. *Nat Methods.* 2012;9:676-682. <https://doi.org/10.1038/nmeth.2019>
 41. Lachmanovich E, Shvartsman DE, Malka Y, Botvin C, Henis YI, Weiss AM. Co-localization analysis of complex formation among membrane proteins by computerized fluorescence microscopy: application to immunofluorescence co-patching studies. *J Microsc.* 2003; 212:122-131. <https://doi.org/10.1046/j.1365-2818.2003.01239.x>
 42. Lagache T, Sauvonnnet N, Danglot L, Olivo-Marin JC. Statistical analysis of molecule colocalization in bioimaging. *Cytom Part A.* 2015;87: 568-579. <https://doi.org/10.1002/cyto.a.22629>
 43. Briggs JAG, Grünwald K, Glass B, Förster F, Kräusslich HG, Fuller SD. The mechanism of HIV-1 core assembly: insights from three-dimensional reconstructions of authentic virions. *Structure.* 2006;14:15-20. <https://doi.org/10.1016/j.str.2005.09.010>
 44. Welsch S, Habermann A, Jäger S, Müller B, Krijnsse-Locker J, Kräusslich HG. Ultrastructural analysis of ESCRT proteins suggests a role for endosome-associated tubular-vesicular membranes in ESCRT function. *Traffic.* 2006;7:1551-1566. <https://doi.org/10.1111/j.1600-0854.2006.00489.x>
 45. Garrus JE, von Schwedler UK, Pornillos OW, et al. Tsg101 and the vacuolar protein sorting pathway are essential for HIV-1 budding. *Cell.* 2001;107:55-65.
 46. VerPlank L, Bouamr F, LaGrassa TJ, et al. Tsg101, a homologue of ubiquitin-conjugating (E2) enzymes, binds the L domain in HIV type 1 Pr55(Gag). *Proc Natl Acad Sci U S A.* 2001;98:7724-7729.
 47. Jouvenet N, Bieniasz PD, Simon SM. Imaging the biogenesis of individual HIV-1 virions in live cells. *Nature.* 2008;454:236-240.
 48. Christ L, Wenzel EM, Liestøl K, Raiborg C, Campsteijn C, Stenmark H. ALIX and ESC RT-I/II function as parallel ESC RT-III recruiters in cyto-kinetic abscission. *J Cell Biol.* 2016;212:499-513.
 49. Wollert T, Hurley JH. Molecular mechanism of multivesicular body biogenesis by ESCRT complexes. *Nature.* 2010;464:864-869.
 50. Goliand I, Nachmias D, Gershony O, Elia N. Inhibition of ESCRT-II-CHMP6 interactions impedes cytokinetic abscission and leads to cell death. *Mol Biol Cell.* 2014;25:3740-3748.
 51. Kutluay SB, Zang T, Blanco-Melo D, et al. Global changes in the RNA binding specificity of HIV-1 gag regulate virion genesis. *Cell.* 2014; 159:1096-1109.
 52. Zhou X, Si J, Corvera J, Gallick GE, Kuang J. Decoding the intrinsic mechanism that prohibits ALIX interaction with ESCRT and viral proteins. *Biochem J.* 2010;432:525-534.
 53. Atilla-Gokcumen GE, Muro E, Relat-Goberna J, et al. Dividing cells regulate their lipid composition and localization. *Cell.* 2014;156:428-439. <https://doi.org/10.1016/j.cell.2013.12.015>
 54. Van Engelenburg SB, Shtengel G, Sengupta P, et al. Distribution of ESCRT machinery at HIV assembly sites reveals virus scaffolding of ESCRT subunits. *Science.* 2014;343:653-656.
 55. Kaye JF, Lever AM. Trans-acting proteins involved in RNA encapsidation and viral assembly in human immunodeficiency virus type 1. *J Virol.* 1996;70:880-886.
 56. Katrukha EA. DoM Utrecht plugins. https://github.com/ekatrakha/DoM_Utrecht.
 57. Cobeldick S. Natural-Order Filename Sort. 2019

58. Tinevez JY, Perry N, Schindelin J, et al. TrackMate: an open and extensible platform for single-particle tracking. *Methods*. 2017;115:80-90. <https://doi.org/10.1016/j.ymeth.2016.09.016>

SUPPORTING INFORMATION

Additional supporting information may be found in the online version of the article at the publisher's website.

How to cite this article: Meng B, Vallejo Ramirez PP, Scherer KM, et al. EAP45 association with budding HIV-1: Kinetics and domain requirements. *Traffic*. 2021;1-15. doi: 10.1111/tra.12820